Tzu Chi Medical Journal 2021; 33 (1): 61–69

Original Article

Multiparametric positron emission tomography/magnetic resonance imaging in nasopharyngeal carcinoma: Correlations between magnetic resonance imaging functional parameters and ^{18}F-fluorodeoxyglucose positron emission tomography imaging biomarkers and their predictive value for treatment failure

Sheng-Chieh Chan[a], Shu-Hang Ng[b], Chih-Hua Yeh[b], Kai-Ping Chang[c]*

[a]Department of Nuclear Medicine, Hualien Tzu Chi Hospital, Buddhist Tzu Chi Medical Foundation, Hualien, Taiwan,[b]Department of Diagnostic Radiology, Linkou Chang Gung Memorial Hospital and Chang Gung University, Taoyuan, Taiwan,[c]Department of Otorhinolaryngology, Linkou Chang Gung Memorial Hospital and Chang Gung University, Taoyuan, Taiwan

Abstract

Objectives: The clinical significance of positron emission tomography/magnetic resonance imaging (PET/MRI) functional parameters in nasopharyngeal carcinoma (NPC) remains unclear. The purpose of this prospective study was two-fold: (1) to investigate the associations between simultaneously acquired PET/MRI perfusion, diffusion, and glucose metabolism parameters in patients with NPC and (2) to analyze their predictive value with respect to treatment failure. **Materials and Methods:** We enrolled 85 patients with primary NPC who simultaneously underwent ^{18}F-fluorodeoxyglucose PET/CT and PET/MRI before definitive treatment. The following variables were determined: (1) functional parameters from the MRI component, including perfusion values (K^{trans}, k_{ep}, v_e, and initial area under the enhancement curve) and apparent diffusion coefficient (ADC) values, and (2) PET parameters, including metabolic tumor volume (MTV). The reciprocal interrelationships between these parameters and their correlations with treatment failure were examined. **Results:** We observed significant negative associations between K^{trans} and ADC ($r = -0.215$, $P = 0.049$) as well as between v_e and ADC ($r = -0.22$, $P = 0.04$). Correlations between PET and MRI functional parameters were not statistically significant. Treatment failures were observed in 21.2% of patients without distant metastases. Multivariate analysis identified v_e as a significant independent predictor for treatment failure ($P = 0.022$), whereas MTV showed a borderline significance ($P = 0.095$). Patients in whom both v_e and MTV values were increased had a significantly higher rate of treatment failure (62.5%) than those with either one (21.9%) or no (7.7%) increased parameter ($P = 0.004$). **Conclusion:** Correlation analyses revealed complex interrelationships among PET and MRI indices measured in patients with NPC. These parameters may have a complementary role in predicting treatment failure in this clinical setting.

Keywords: *DCE-MRI, Diffusion-weighted MRI, Nasopharyngeal carcinoma, Positron emission tomography/magnetic resonance imaging, Prognosis*

Submission : 08-Jan-2020
Revision : 10-Feb-2020
Acceptance : 27-Feb-2020
Web Publication : 10-Apr-2020

Introduction

Nasopharyngeal carcinoma (NPC) differs significantly from other head and neck squamous cell carcinomas (HNSCCs) in terms of histological characteristics, treatment strategies, and clinical course [1]. There is also a distinctive geographic distribution of this malignancy in Southeast Asia and Northeastern Africa [1]. Despite recent advances in the field of radiotherapy or chemoradiotherapy, the survival of patients with NPC remains suboptimal [2].

Both magnetic resonance imaging (MRI) and ^{18}F-fluorodeoxyglucose positron emission tomography/computed tomography (^{18}F-FDG-PET/CT) are currently part of

Supplementary material available online

Access this article online

Quick Response Code:

Website: www.tcmjmed.com

DOI: 10.4103/tcmj.tcmj_4_20

**Address for correspondence*
Dr. Shu-Hang Ng,
Department of Diagnostic Radiology, Linkou Chang Gung Memorial Hospital, 5, Fuxing Street, Guishan District, Taoyuan, Taiwan.
E-mail: shuhangng@gmail.com

How to cite this article: Chan SC, Ng SH, Yeh CH, Chang KP. Multiparametric positron emission tomography/magnetic resonance imaging in nasopharyngeal carcinoma: Correlations between magnetic resonance imaging functional parameters and ^{18}F-fluorodeoxyglucose positron emission tomography imaging biomarkers and their predictive value for treatment failure. Tzu Chi Med J 2021; 33(1): 61-9.

the staging workup of NPC [1,3]. Besides anatomic information, MRI allows performing functional imaging, including the analysis of tumor perfusion with dynamic contrast-enhanced MRI (DCE-MRI) and the assessment of tumor cellularity using diffusion-weighted imaging (DWI).

A recent study demonstrated that DCE-MRI-derived perfusion parameters may predict treatment response in patients with NPC treated with neoadjuvant chemoradiotherapy [4]. In addition, it has been previously shown that a high pretreatment apparent diffusion coefficient (ADC) on DWI is associated with a poor response to treatment and unfavorable posttherapeutic survival figures in different solid malignancies, including NPC [5] and breast cancer [6]. The ability of ^{18}F-FDG PET/CT to predict treatment response and clinical outcomes in patients with NPC has been consistently demonstrated [7,8].

Different tumor characteristics (e.g., perfusion, cellularity, and glucose metabolism) are characterized by complex interrelationships, which, if understood in greater detail, can inform treatment planning and improve prognostic stratification. Integrated PET/MRI allows the simultaneous assessment of both PET glucose metabolism and MRI parameters of tumor perfusion/cellularity. The application of ^{18}F-FDG PET/MRI for NPC staging is clinically feasible [9]. Cheng *et al*. [10] have also described the association between PET/CT and PET/MRI parameters. However, PET/MRI in their study [10] was obtained by the fusion of images from separate PET and MRI machines. In a small-sized study conducted in patients with NPC (n = 21), Cao *et al*. [11] have previously explored the feasibility of multiparametric imaging using an integrated PET/MRI scanner. However, the question as to whether these parameters can have prognostic significance in patients with NPC remains open.

In this scenario, the purpose of this prospective study was two-fold: (1) to investigate the associations between simultaneously acquired PET/MRI perfusion, diffusion, and glucose metabolism parameters in patients with NPC and (2) to analyze their predictive value with respect to treatment failure.

Materials and methods

Ethics statements

The study protocol complied with the tenets of the Helsinki Declaration. Ethical approval was granted by the Institutional Review Board of Chang Gung Memorial Hospital (IRB no. 103-7498A3) and all participants provided their written informed consent.

Study patients and clinical management

Patients with a histological diagnosis of primary NPC, no contraindications to MRI, and serum glucose levels <150 mg/dL before ^{18}F-FDG PET/CT imaging were deemed eligible. Exclusion criteria were renal failure, claustrophobia, or other general contraindications to MRI.

On the same day, all of the study participants underwent ^{18}F-FDG PET/CT followed by whole-body ^{18}F-FDG PET/MRI. Patients with Stage I disease received definitive radiation therapy alone, whereas those with Stage II–IVB disease were treated with concurrent chemoradiotherapy. Standard platinum-based chemotherapy was administered to patients with metastatic disease [12,13].

Supplementary Figure 1 depicts the flow of patients through the study. Between October 2015 and May 2017, we identified 104 potentially eligible patients with primary NPC. Of them, four were excluded because they met at least one exclusion criteria. The remaining 100 patients underwent both ^{18}F-FDG PET/CT and ^{18}F-FDG PET/MRI imaging using the DWI and DCE-MRI protocols. The mean time interval between the scans was 61 min. Fifteen patients had MRI data not assessable either because of prominent motion artifacts or the presence of small-sized tumors. Consequently, the final study sample consisted of 85 patients [Table 1].

^{18}F-fluorodeoxyglucose positron emission tomography/computed tomography

Patients were required to fast for at least 6 h before ^{18}F-FDG PET/CT imaging on a Biograph mCT scanner (Siemens Medical Solutions, Malvern, PA, USA), which comprises a four-ring PET scanner and a 40-section CT scanner. Between 50 and 70 min after injection of ^{18}F-FDG (370 MBq), PET emission images were obtained from the vertex to the mid-thigh. The scanning time per table position was 1.5 min, and a 200 × 200 matrix size was used. Before PET acquisition, patients underwent a standard helical CT imaging (from the head to the proximal thigh) using the manufacturer-supplied dose reduction software CareKV and CareDose 4D. The

Table 1: General characteristics of the study patients (n=85)

Characteristic	n
Sex	
Male	61
Female	24
Age (years), mean±SD	51±13
T status	
T1	17
T2	16
T3	27
T4	25
N status	
N0	8
N1	38
N2	17
N3	22
M status	
M0	76
M1	9
AJCC/UICC stage (7th ed..ition)	
I	3
II	17
III	23
IV	42
Cell type	
WHO I	1
WHO II	13
WHO III	71

AJCC: American Joint Committee on Cancer, UICC: Union for International Cancer Control, WHO: World Health Organization

following parameters were used: preset, 120 kV; collimation, 40 × 0.6 mm; pitch, 1.5; slice thickness, 2 mm. No intravenous iodinated contrast agents were administered. PET images were reconstructed with CT data for attenuation correction using an ordered-subset expectation maximization iterative reconstruction algorithm (2 iterations, 21 subsets).

^{18}F-fluorodeoxyglucose positron emission tomography/magnetic resonance imaging

Upon PET/CT completion, PET/MRI was performed on an integrated PET/MRI scanner (Biograph mMR, Siemens Healthcare, Erlangen, Germany), which simultaneously acquires PET and MRI data using a 3.0-T magnet. The examination protocol consisted of a whole-body scan followed by a detailed examination of the head and neck area [Supplementary Table 1]. We initially acquired a fast-view T1-weighted MRI localizer sequence for scout imaging and a Dixon volumetric interpolated breath-hold examination (VIBE) sequence for attenuation correction. Subsequently, a whole-body PET scan was performed from the head to the proximal thigh in four-bed positions (acquisition time per bed position: 4 min). During PET data acquisition, whole-body MRI was conducted simultaneously (for the corresponding four bed positions) using an axial breath-holding half-Fourier single-shot turbo spin echo (TSE) sequence and a sagittal short tau inversion recovery sequence.

Thereafter, regional head and neck PET and MRI images were obtained simultaneously. PET was performed with an acquisition time of 10 min, whereas MRI was acquired in the axial and coronal projections with a T1-weighted TSE sequence and a T2-weighted TSE sequence with fat saturation. Regional DWI was acquired using single-shot spin-echo echo-planar imaging with the modified Stejskal–Tanner diffusion gradient pulsing scheme. Coverage and image slicing were identical for T1- and T2-weighted images. Motion-probing gradients (b-value: 800 s/mm^2) were applied along three orthogonal directions.

DCE-MRI of the head and neck region was subsequently acquired using a three-dimensional T1-weighted spoiled gradient-echo sequence. Before administration of the contrast agent, baseline longitudinal relaxation time ($T1_0$) values were calculated from the acquired images with the application of different flip angles (4°, 8°, 15°, and 25°). Dynamic series were obtained using the same sequence (flip angle: 15°) after the intravenous administration of a paramagnetic contrast agent (injection rate: 3 mL/s). Dedicated regional MRI imaging of the head and neck was carried out using a T1-weighted TSE sequence with fat saturation in the axial and coronal projections. We finally performed a whole-body axial VIBE with fat saturation. PET data were reconstructed using an ordinary Poisson ordered subset expectation maximization, with three iterations, 21 subsets, and a 4-mm Gaussian postprocessing filter into 344 × 344 matrices.

Image analysis

DCE-MRI images were transferred onto a postprocessing workstation and were analyzed using dedicated software (TISSUE 4D, Siemens Medical Systems, Erlangen, Germany). After motion correction and registration of pre- and postcontrast acquisitions, T1 mapping was generated automatically. Freehand regions of interest (ROIs) were manually drawn by an experienced head and neck radiologist in the primary tumor area. The software allows the implementation of a population-based approach for arterial input function, which was scaled in relation to the gadolinium dose and modeled with the biexponential method proposed by Tofts *et al*. and Kermode [14]. The pharmacokinetic parameters K^{trans}, K_{ep}, $v_{e,}$ and initial area under the enhancement curve (iAUC) were subsequently calculated. In the two-compartment model, the volume transfer constant K^{trans} reflects the efflux rate of the contrast medium from blood plasma into the interstitial space through the vessel wall. v_e is a measure of extravascular extracellular leakage space (ELS) volume. K_{ep} reflects the backward flux of the contrast medium from the ELS to the blood plasma. The iAUC is related to the volume of blood in the tissue of interest. In this study, iAUC refers to the initial area under the time-concentration curve defined over the first 60 s of postenhancement images. DWI-derived ADC values were measured on ADC maps by drawing the ROI on tumors. A senior head and neck radiologist performed the procedure with the aid of T2-weighted and contrast-enhanced T1-weighted images.

The PMOD software package (PMOD Technologies Ltd., Zurich, Switzerland) was used to calculate ^{18}F-FDG PET parameters. All of the ROIs were manually drawn by an experienced nuclear medicine physician. Standardized uptake value (SUV) was determined using the following formula: SUV = (decay-corrected activity in kilobecquerels per milliliter of tissue volume)/(injected FDG activity in kilobecquerels/body weight in grams). MTV was obtained from attenuation-corrected ^{18}F-FDG PET images. Boundaries were drawn large enough to include the primary nasopharyngeal tumor. In keeping with previous methodology [8,12,15], we used a SUV cutoff value of 2.5 to automatically generate contour margins around the target and within the boundary. All of the voxels with SUV values >2.5 within the contour margin were considered to calculate the MTV. We also determined the mean SUV value within the contour margin. Finally, total lesion glycolysis (TLG) was calculated as follows: TLG = Mean SUV × MTV.

Follow-up schedule and identification of treatment failure

Patients were followed every week during the course of treatment and then every 3 months for the first 2 years, every 4 months for the subsequent 2 years, and every 6 months thereafter. A conventional workup was performed 3 months after treatment completion and subsequently either on a yearly basis or when clinically indicated. A lesion suspected of being a treatment failure was subjected to endoscopic biopsy, ultrasound-guided fine-needle aspiration, or CT-guided biopsy. When a biopsy was unfeasible or yielded a negative result, the patient underwent a close clinical and imaging follow-up.

Statistical analysis

Patients were followed up until January 2019 or censored on the date of death. The associations between the study variables were investigated using the Pearson's correlation coefficient, whereas the Chi-square test was used to analyze the relationships between different clinical and imaging

parameters and treatment failures. Continuous clinical and imaging variables were dichotomized according to their mean values. Independent predictors of treatment failures were identified using multivariate analysis. Statistical calculations were performed with the SPSS statistical package (version 21.0; SPSS Inc., Chicago, IL, USA). Two-tailed $P < 0.05$ was considered statistically significant.

Results

Correlation between different imaging parameters

The values of PET and MRI imaging parameters are shown in Supplementary Table 2. We found highly significant positive correlations between SUV, MTV, and TLG values measured on PET/CT and PET/MRI [$P < 0.001$, Supplementary Table 3]. As far as PET/MRI parameters are concerned, there were significant positive correlations [Figure 1a and Table 2] between K^{trans} and k_{ep} ($r = 0.907$, $P < 0.001$), K^{trans} and v_e ($r = 0.416$, $P < 0.001$), as well as K^{trans} and iAUC ($r = 0.601$, $P < 0.001$). Other significant positive correlations were those between k_{ep} and v_e, k_{ep} and iAUC, as well as v_e and iAUC. Conversely, significant inverse correlations were evident between K^{trans} and ADC [$r = -0.215$, $P = 0.049$, Figure 1b] as well as v_e and ADC ($r = -0.22$, $P = 0.049$). DCE-MRI parameters and ADC did not show any significant correlation with SUV, MTV, or TLG [Figure 1c].

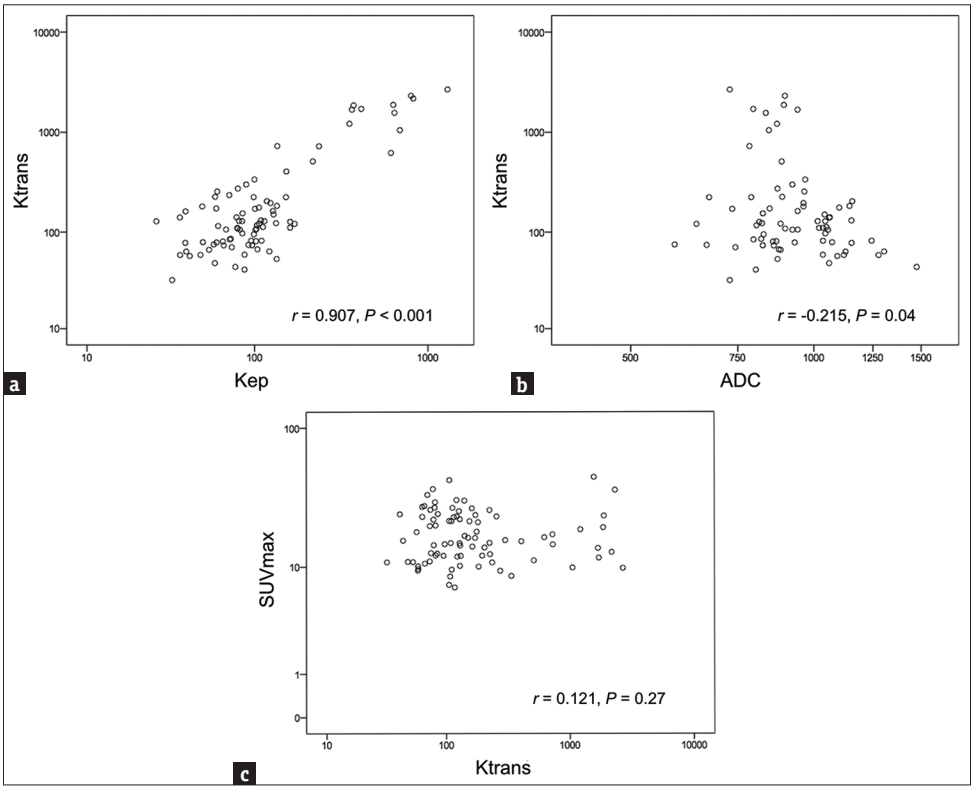

Figure 1: Correlations between different PET/MRI functional parameters.Scatter diagrams showing the distribution of PET/MRI K^{trans} in relation to k_{ep} (panel a), ADC (panel b), and SUV_{max} (panel c). PET/MRI: Positron emission tomography/magnetic resonance imaging, ADC: Apparent diffusion coefficient, SUV_{max}: Maximum standardized uptake volume

Table 2: Correlation analysis of different dynamic contrast-enhanced magnetic resonance imaging, diffusion-weighted imaging, and ^{18}F-fluorodeoxyglucose positron emission tomography parameters measured on positron emission tomography/magnetic resonance imaging

	r (P)				
	K^{trans}	k_{ep}	v_e	iAUC	ADC
SUV_{max}	0.121 (0.270)	0.100 (0.361)	−0.011 (0.918)	0.047 (0.671)	−0.063 (0.568)
MTV	0.093 (0.398)	0.083 (0.450)	0.004 (0.972)	−0.001 (0.996)	0.077 (0.481)
TLG	0.127 (0.246)	0.138 (0.208)	0.003 (0.982)	0.011 (0.917)	0.013 (0.906)
k_{ep}	0.907 (<0.001)				
v_e	0.416 (<0.001)	0.248 (0.022)			
iAUC	0.601 (<0.001)	0.435 (<0.001)	0.516 (<0.001)		
ADC	−0.215 (0.049)	−0.179 (0.101)	−0.220 (0.049)	−0.168 (0.125)	

SUV_{max}: Maximum standardized uptake volume, MTV: Metabolic tumor volume, TLG: Total lesion glycolysis, iAUC: Initial area under the enhancement curve, K^{trans}: Volume transfer constant, k_{ep}: Flux rate constant, v_e: Extracellular volume ratio, ADC: Apparent diffusion coefficient

Prediction of treatment failure using positron emission tomography/magnetic resonance imaging functional parameters

PET/MRI functional parameters were analyzed in relation to treatment failure [Table 3]. Of the 76 patients without distant metastases, ten were lost to follow-up [Supplementary Figure 1]. Consequently, the analysis was conducted on 66 patients. Treatment failures were identified in 14 (21.2%) cases. Specifically, locoregional, distant, and both locoregional and distant failures were diagnosed in 4, 7, and 3 patients, respectively. Male sex (P = 0.006), T3-4 status (P = 0.016), N2-3 status (P = 0.032), and higher AJCC staging (P = 0.007) were significant predictors for treatment failures. MTV from PET and v_e from DCE-MRI were capable of distinguishing between patients who developed treatment failures from those who did not [P = 0.049 and 0.045, respectively, Figure 2]. After allowance for potential confounders in multivariate analysis, v_e was retained in the model as the only significant independent predictor of treatment failure (P = 0.022, hazard ratio = 6.495), whereas MTV showed a borderline significance (P = 0.095, hazard ratio = 3.914). Patients with an increase in both v_e and MTV had a significantly higher recurrence rate [62.5%, 5/8; Figure 3] than those with either one (21.9%, 7/32) or no (7.7%) increased parameter (P = 0.004). Two illustrative cases without and with treatment failures and their corresponding PET and MRI parametric images are shown in Figures 4 and 5.

The sensitivity, specificity, and area under curve (AUC) of v_e>296 and MTV >14 in the prediction of treatment failures were 64.29%, 65.38%, and 0.622 and 57.14%, 75%, and 0.640, respectively. Supplementary Table 4 shows the diagnostic properties of different imaging parameters.

Male sex (P = 0.026), N2-3 status (P = 0.041), higher EBV DNA titer (P = 0.02), higher K^{trans} (P = 0.02), or k_{ep} (P = 0.013) were significant predictors for distant failures. After allowance for potential confounders in multivariate analysis, kep was retained in the model as the only significant independent predictor (P = 0.018).

Table 3: Univariate analysis for predictors of treatment failure in patients with primary M0 nasopharyngeal carcinoma

Variable	*n* (%)	Treatment failure	
		n	*P*
Patient number	66	14	
Age (years)			
≤50	31 (47)	6	0.728
>50	35 (53)	8	
Sex			
Female	20 (30)	0	0.006
Male	46 (79)	14	
Cell type			
WHO Type I	2 (3)	1	0.194
WHO Type II	8 (12)	0	
WHO Type III	56 (85)	13	
T status			
T1-2	28 (42)	2	0.016
T3-4	38 (58)	12	
N status			
N0-1	40 (61)	5	0.032
N2-3	26 (39)	9	
AJCC/UICC stage			
Stage I-II	18 (27)	0	0.007
Stage III-IVb	48 (73)	14	
EBV DNA (copies/mL)			
≤5700	53 (80)	9	0.097
>5700	13 (20)	5	
SUV_{max} (g/mL)			
≤18.9	36 (55)	6	0.322
>18.9	30 (45)	8	
MTV (mL)			
≤14	45 (68)	6	0.049
>14	21 (32)	8	
$K^{trans} \times 10^3$ (min^{-1})			
≤380	53 (80)	9	0.128
>380	13 (20)	5	
$k_{ep} \times 10^3$ (min^{-1})			
≤180	54 (52)	9	0.111
>180	12 (48)	5	
$v_e \times 10^3$			
≤296	39 (59)	5	0.045
>296	27 (41)	9	
iAUC (mm^2/s)			
≤1000	38 (58)	8	0.971
>1000	28 (42)	6	
ADC (mm^2/s)			
≤767	18 (27)	2	0.318
>767	48 (73)	12	

WHO: World Health Organization, AJCC: American Joint Committee on Cancer, UICC: Union for International Cancer Control, EBV: Epstein-Barr virus, SUVmax: Maximum standardized uptake volume, MTV: Metabolic tumor volume, iAUC: Initial area under the enhancement curve, K^{trans}: Volume transfer constant, K_{ep}: Flux rate constant, v_e: extracellular volume ratio, ADC: Apparent diffusion coefficient

Discussion

The main findings of our study are as follows: (1) simultaneous ^{18}F-FDG-PET/MRI is clinically feasible in patients with NPC, with indices of tumor perfusion, tissue metabolism, and cellularity being successfully acquired in this malignancy; (2) MRI perfusion parameters are correlated with the diffusion parameter ADC, but no significant correlation exists between PET and MRI parameters; and (3) v_e and MTV may serve as biomarkers of treatment failures. Taken together, our results indicate that different imaging biomarkers derived from simultaneously acquired PET/MRI may provide complementary information in the pathogenesis of NPC and in the prediction of treatment failures in patients with primary NPC. To our knowledge, this is the first report describing the prognostic utility of PET/MRI parameters in NPC.

ADC values are increasingly being used as a diagnostic adjunct in the imaging workup of patients with suspected malignancies [16,17]. Conversely, DCE-MRI has emerged as a valuable technique for investigating the properties of tissue microvasculature. Using a 3.0 T MRI scanner, Ni and Liu [18] have reported negative correlations between ADC and DCE-MRI parameters (K^{trans}, $k_{ep,}$ or v_e) in 44 patients with NPC. In keeping with their findings, we identified a significant

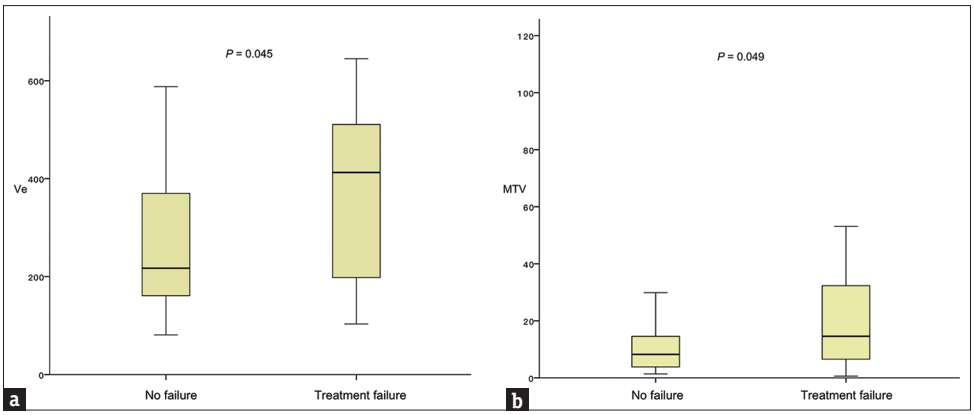

Figure 2: Boxplots of v_e (a) and MTV (b) categorized by treatment failure status. MTV: Metabolic tumor volume

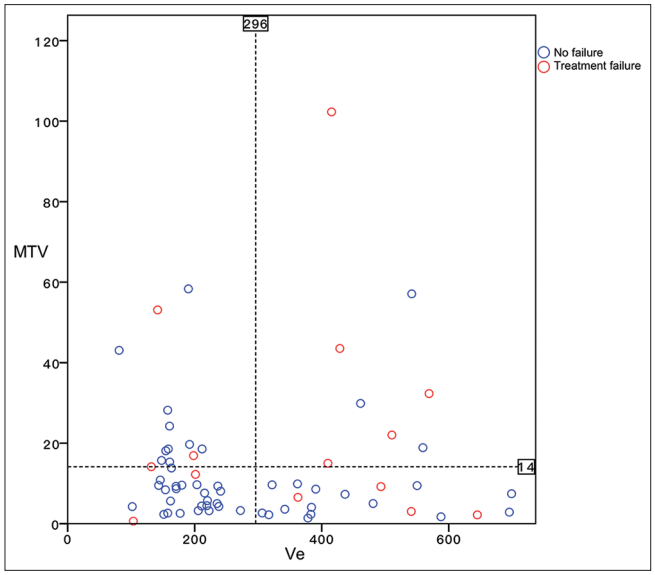

Figure 3: Dot plots of v_e against MTV categorized by treatment failure status. The horizontal dashed line on the Y-axis indicates the mean v_e value, whereas the vertical dashed line on the X-axis denotes the mean MTV value. Patients with a concomitant increase in both MTV and v_e were characterized by a markedly higher rate of failures compared with those with either one or no increased parameter ($P = 0.004$). MTV: Metabolic tumor volume

negative association between ADC and K^{trans} or v_e. These results may be explained by the higher cellularity, increased cellular size, and elevated microvessel density and permeability of malignant nasopharyngeal tissue.

Previous studies conducted in patients with cervical, lung, rectal, and breast malignancies have generally shown a significant inverse correlation between FDG metabolism and ADC [19-23]. However, some studies conducted in HNSCCs have failed to confirm this relationship [24-26]. As far as NPC is concerned, two recent investigations failed to identify a significant correlation between SUV and ADC [10,11]. In the current study, we found no association between ADC and SUV [$P = 0.568$, Table 2], confirming that these biomarkers are unrelated with each other in patients with NPC. ADC quantification is prone to variations caused by different lesion components, neoplasm size, field strength, and selection of b-values [27], ultimately resulting in inconsistent associations between ADC and SUV in different malignancies.

A limited number of studies examined the relationships between DCE-MRI and ^{18}F-FDG PET indices. No correlation between glucose metabolic parameters and K^{trans} or k_{ep} has been identified in patients with HNSCCs [28,29], a finding confirmed in our study focusing on NPC. In light of these results, PET and DCE-MRI parameters seem to be unrelated with each other.

The use of multiparametric PET/MRI imaging for predicting prognosis in patients with malignancies is gaining momentum. In a study conducted using separate PET/CT and MRI scanners, Ng *et al*. [30] demonstrated that k_{ep}, v_e, and SUV were independent predictors of survival in patients with hypopharyngeal or oropharyngeal carcinoma. Wong *et al*. [31] reported that changes in SUV, TLG, or MRI-derived v_e, K^{trans}, ADC from separate PET and MRI scanners are significant predictors of treatment response in patients with HNSCC [31]. These promising results notwithstanding, the clinical utility of multiparametric PET and MRI imaging remains unclear in NPC. In the current study, v_e and MTV were associated with treatment failures in patients with primary NPC. MTV, which reflects the burden of tracer-avid tumor tissue, has been shown to predict disease recurrences in NPC and other HNSCCs [32-34]. v_e is a parameter reflecting the amount of extravascular extracellular space. Most neoplasms are characterized by high v_e values, which may serve as a proxy for tumor aggressiveness [35]. Previous reports have shown that v_e is associated with prognosis and treatment outcomes in HNSCC [30,31] and colorectal cancer [36]. Moreover, Chin *et al*. [37] described a positive association between v_e and the occurrence of early distant metastases in NPC. Our study, based on the use of integrated PET/MRI, further demonstrates that v_e is a significant risk factor for tumor relapse in patients with NPC. Notably, the combined assessment of both MTV and v_e may allow patients to be stratified into three distinct prognostic groups. Accordingly, we observed that the rate of treatment failure of subjects with a concomitant increase in both MTV and v_e was markedly higher (62.5%) than that of patients with either one (21.9%) or no (7.7%) increased parameter. Patients characterized by an increased risk of tumor relapse (i.e., with concomitant increase in both MTV and v_e) may be suitable

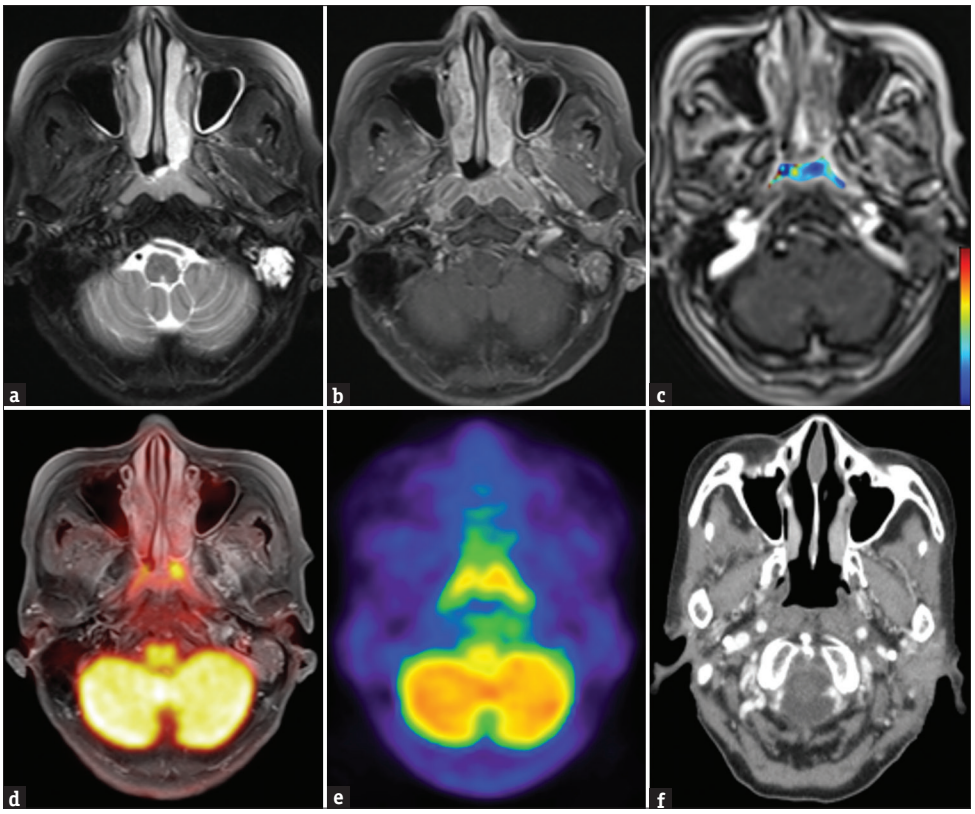

Figure 4: A 77-year-old woman with T4N2M0 NPC. T2-weighted (panel a) and contrast-enhanced T1-weighted images (panel b) revealed the presence of a primary nasopharyngeal neoplasm. The corresponding DCE-MRI image with an overlaid v_e map (panel c) showed a low value (240.79). According to ^{18}F-FDG PET/MRI (panel d) and PET (panel e) images, the metabolic tumor volume was 8.06. The patient was treated with definitive concurrent chemoradiotherapy. After 2 years of treatment, she is alive without relapses (panel f). The patient had low values of both v_e and MTV. NPC: Nasopharyngeal carcinoma, DCE: Dynamic contrast-enhanced, MRI: Magnetic resonance imaging, PET: Positron emission tomography, ^{18}F-FDG: ^{18}F-fluorodeoxyglucose, MTV: Metabolic tumor volume

candidates to receive induction chemotherapy or more strict surveillance protocols in future clinical trials.

It is noteworthy that the vast majority of studies focusing on the utility of multimodality imaging in the prognostic stratification of patients with head and neck malignancies have been performed using separate PET and MRI scanners [30,31,37]. In this scenario, we believe that simultaneous integrated PET/MRI imaging can outperform separate scans in terms of patient acceptability and minimize the biological variation related to distinct systems.

With regard to the applications of PET/MRI in current clinical practice, Chan *et al*. [9] have previously compared the diagnostic performances of PET/MRI and PET/CT for staging of primary NPC. By increasing the conspicuity of morphologically subtle lesions, PET/MR imaging may map local tumor extension more precisely than PET/CT. Moreover, PET/MRI also has a higher accuracy in the assessment of regional nodal status and an increased positive predictive value for distant metastases. Compared with PET/CT, PET/MRI allows obtaining an accurate disease staging in a single step with an excellent imaging co-registration. However, PET/MRI is not without limitations, including a low availability, high costs, and a longer scan length.

Some limitations of our study merit comment. First, our research was a single-center investigation. Second, longer follow-up periods are required to identify reliable predictors of long-term survival. Third, the analytical model for DCE-MRI and DWI used in this study might not be applicable to all patients, especially in the presence of small-sized or cystic lesions.

Conclusion

Different correlations between PET/MRI functional parameters identified in our study indicate that NPC is characterized by complex interrelationships between indices of metabolism, perfusion, and cellularity. It is thus possible that these parameters reflect different facets of NPC pathogenesis. MTV measured on PET and v_e assessed by DCE-MRI were identified as predictors of treatment failures and their combination allowed patient stratification into three distinct prognostic groups. PET and MRI perfusion imaging biomarkers derived from PET/MRI may have a complementary role in predicting treatment failure in patients with primary NPC.

Acknowledgments

The authors are thankful to Jhih-Chao Yang for his help in PET data processing.

Financial support and sponsorship

This work was supported in part by the Taiwan Ministry of Science and Technology (grant NSC 104-2314-B-182A-084-MY3).

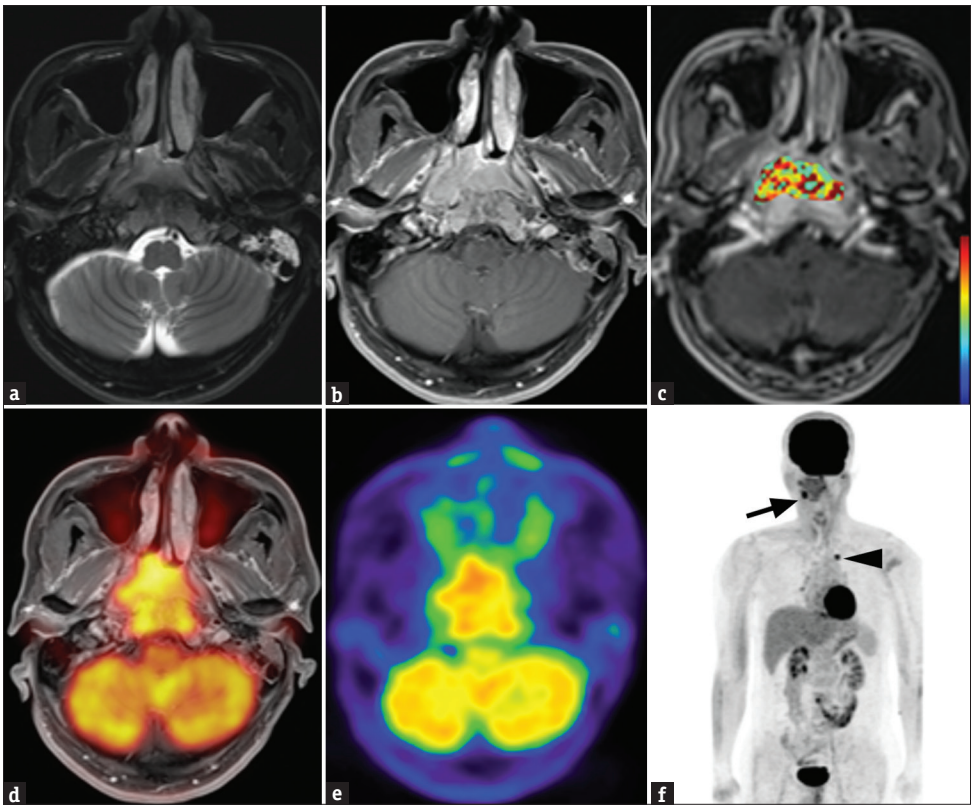

Figure 5: A 47-year-old male with T4N2M0 NPC. T2-weighted (panel a) and contrast-enhanced T1-weighted images (panel b) revealed the presence of a primary nasopharyngeal neoplasm. The corresponding DCE-MRI image with an overlaid v_e map (panel c) showed a high value (569.02). According to PET (panel e) and PET/MRI (panel d) images, the metabolic tumor volume was 32.31. The patient was treated with definitive concurrent chemoradiotherapy. After 1 year, treatment failures were identified in a neck lymph node (arrow) and at the ribs (arrowhead; panel f). High values of both v_e and MTV were noted in this patient. NPC: Nasopharyngeal carcinoma, DCE: Dynamic contrast-enhanced, MRI: Magnetic resonance imaging, PET: Positron emission tomography, MTV: Metabolic tumor volume

Conflicts of interest

There are no conflicts of interest.

References

1. Chua ML, Wee JT, Hui EP, Chan AT. Nasopharyngeal carcinoma. Lancet 2016;387:1012-24.
2. O'Sullivan B. Nasopharynx cancer: Therapeutic value of chemoradiotherapy. Int J Radiat Oncol Biol Phys 2007;69:S118-21.
3. Ng SH, Chan SC, Yen TC, Chang JT, Liao CT, Ko SF, et al. Staging of untreated nasopharyngeal carcinoma with PET/CT: Comparison with conventional imaging work-up. Eur J Nucl Med Mol Imaging 2009;36:12-22.
4. Zheng D, Yue Q, Ren W, Liu M, Zhang X, Lin H, et al. Early responses assessment of neoadjuvant chemotherapy in nasopharyngeal carcinoma by serial dynamic contrast-enhanced MR imaging. Magn Reson Imaging 2017;35:125-31.
5. Zhang Y, Liu X, Zhang Y, Li WF, Chen L, Mao YP, et al. Prognostic value of the primary lesion apparent diffusion coefficient (ADC) in nasopharyngeal carcinoma: A retrospective study of 541 cases. Sci Rep 2015;5:12242.
6. Park SH, Moon WK, Cho N, Song IC, Chang JM, Park IA, et al. Diffusion-weighted MR imaging: Pretreatment prediction of response to neoadjuvant chemotherapy in patients with breast cancer. Radiology 2010;257:56-63.
7. Chan SC, Chang JT, Wang HM, Lin CY, Ng SH, Fan KH, et al. Prediction for distant failure in patients with stage M0 nasopharyngeal carcinoma: The role of standardized uptake value. Oral Oncol 2009;45:52-8.
8. Xie P, Yue JB, Zhao HX, Sun XD, Kong L, Fu Z, et al. Prognostic value of 18F-FDG PET-CT metabolic index for nasopharyngeal carcinoma. J Cancer Res Clin Oncol 2010;136:883-9.
9. Chan SC, Yeh CH, Yen TC, Ng SH, Chang JT, Lin CY, et al. Clinical utility of simultaneous whole-body (18)F-FDG PET/MRI as a single-step imaging modality in the staging of primary nasopharyngeal carcinoma. Eur J Nucl Med Mol Imaging 2018;45:1297-308.
10. Cheng Y, Bai L, Shang J, Tang Y, Ling X, Guo B, et al. Preliminary clinical results for PET/MR compared with PET/CT in patients with nasopharyngeal carcinoma. Oncol Rep 2020;43:177-87.
11. Cao C, Yang P, Xu Y, Niu T, Hu Q, Chen X. Feasibility of multiparametric imaging with PET/MR in nasopharyngeal carcinoma: A pilot study. Oral Oncol 2019;93:91-5.
12. Chan SC, Hsu CL, Yen TC, Ng SH, Liao CT, Wang HM. The role of 18F-FDG PET/CT metabolic tumour volume in predicting survival in patients with metastatic nasopharyngeal carcinoma. Oral Oncol 2013;49:71-8.
13. Chang KP, Tsang NM, Liao CT, Hsu CL, Chung MJ, Lo CW, et al. Prognostic significance of 18F-FDG PET parameters and plasma Epstein-Barr virus DNA load in patients with nasopharyngeal carcinoma. J Nucl Med 2012;53:21-8.
14. Tofts PS, Berkowitz B, Schnall MD. Quantitative analysis of dynamic Gd-DTPA enhancement in breast tumors using a permeability model. Magn Reson Med 1995;33:564-8.
15. Chen YH, Chang KP, Chu SC, Yen TC, Wang LY, Chang JT, et al. Value of early evaluation of treatment response using (18)F-FDG PET/CT parameters and the Epstein-Barr virus DNA load for prediction of outcome in patients with primary nasopharyngeal carcinoma. Eur J Nucl Med Mol Imaging 2019;46:650-60.
16. Kim JK, Kim KA, Park BW, Kim N, Cho KS. Feasibility of

diffusion-weighted imaging in the differentiation of metastatic from nonmetastatic lymph nodes: Early experience. J Magn Reson Imaging 2008;28:714-9.

17. Koh DM, Collins DJ. Diffusion-weighted MRI in the body: Applications and challenges in oncology. AJR Am J Roentgenol 2007;188:1622-35.
18. Ni L, Liu Y. Contrast-enhanced dynamic and diffusion-weighted magnetic resonance imaging at 3.0 T to assess early-stage nasopharyngeal carcinoma. Oncol Lett 2018;15:5294-300.
19. Gu J, Khong PL, Wang S, Chan Q, Law W, Zhang J. Quantitative assessment of diffusion-weighted MR imaging in patients with primary rectal cancer: Correlation with FDG-PET/CT. Mol Imaging Biol 2011;13:1020-8.
20. Ho KC, Lin G, Wang JJ, Lai CH, Chang CJ, Yen TC. Correlation of apparent diffusion coefficients measured by 3T diffusion-weighted MRI and SUV from FDG PET/CT in primary cervical cancer. Eur J Nucl Med Mol Imaging 2009;36:200-8.
21. Nakajo M, Kajiya Y, Kaneko T, Kaneko Y, Takasaki T, Tani A, et al. FDG PET/CT and diffusion-weighted imaging for breast cancer: Prognostic value of maximum standardized uptake values and apparent diffusion coefficient values of the primary lesion. Eur J Nucl Med Mol Imaging 2010;37:2011-20.
22. Regier M, Derlin T, Schwarz D, Laqmani A, Henes FO, Groth M, et al. Diffusion weighted MRI and 18F-FDG PET/CT in non-small cell lung cancer (NSCLC): Does the apparent diffusion coefficient (ADC) correlate with tracer uptake (SUV)? Eur J Radiol 2012;81:2913-8.
23. Schmidt H, Brendle C, Schraml C, Martirosian P, Bezrukov I, Hetzel J, et al. Correlation of simultaneously acquired diffusion-weighted imaging and 2-deoxy-[18F] fluoro-2-D-glucose positron emission tomography of pulmonary lesions in a dedicated whole-body magnetic resonance/positron emission tomography system. Invest Radiol 2013;48:247-55.
24. Choi SH, Paeng JC, Sohn CH, Pagsisihan JR, Kim YJ, Kim KG, et al. Correlation of 18F-FDG uptake with apparent diffusion coefficient ratio measured on standard and high b value diffusion MRI in head and neck cancer. J Nucl Med 2011;52:1056-62.
25. Fruehwald-Pallamar J, Czerny C, Mayerhoefer ME, Halpern BS, Eder-Czembirek C, Brunner M, et al. Functional imaging in head and neck squamous cell carcinoma: Correlation of PET/CT and diffusion-weighted imaging at 3 Tesla. Eur J Nucl Med Mol Imaging 2011;38:1009-19.
26. Varoquaux A, Rager O, Lovblad KO, Masterson K, Dulguerov P, Ratib O, et al. Functional imaging of head and neck squamous cell carcinoma with diffusion-weighted MRI and FDG PET/CT: Quantitative analysis of ADC and SUV. Eur J Nucl Med Mol Imaging 2013;40:842-52.
27. Connolly M, Srinivasan A. Diffusion-Weighted Imaging in Head and Neck Cancer: Technique, Limitations, and Applications. Magn Reson Imaging Clin N Am 2018;26:121-33.
28. Bisdas S, Seitz O, Middendorp M, Chambron-Pinho N, Bisdas T, Vogl TJ, et al. An exploratory pilot study into the association between microcirculatory parameters derived by MRI-based pharmacokinetic analysis and glucose utilization estimated by PET-CT imaging in head and neck cancer. Eur Radiol 2010;20:2358-66.
29. Jansen JF, Schöder H, Lee NY, Stambuk HE, Wang Y, Fury MG, et al. Tumor metabolism and perfusion in head and neck squamous cell carcinoma: Pretreatment multimodality imaging with 1H magnetic resonance spectroscopy, dynamic contrast-enhanced MRI, and [18F] FDG-PET. Int J Radiat Oncol Biol Phys 2012;82:299-307.
30. Ng SH, Liao CT, Lin CY, Chan SC, Lin YC, Yen TC, et al. Dynamic contrast-enhanced MRI, diffusion-weighted MRI and (18)F-FDG PET/CT for the prediction of survival in oropharyngeal or hypopharyngeal squamous cell carcinoma treated with chemoradiation. Eur Radiol 2016;26:4162-72.
31. Wong KH, Panek R, Dunlop A, Mcquaid D, Riddell A, Welsh LC, et al. Changes in multimodality functional imaging parameters early during chemoradiation predict treatment response in patients with locally advanced head and neck cancer. Eur J Nucl Med Mol Imaging 2018;45:759-67.
32. Chan SC, Chang JT, Lin CY, Ng SH, Wang HM, Liao CT, et al. Clinical utility of 18F-FDG PET parameters in patients with advanced nasopharyngeal carcinoma: Predictive role for different survival endpoints and impact on prognostic stratification. Nucl Med Commun 2011;32:989-96.
33. Chung MK, Jeong HS, Park SG, Jang JY, Son YI, Choi JY, et al. Metabolic tumor volume of [18F]-fluorodeoxyglucose positron emission tomography/computed tomography predicts short-term outcome to radiotherapy with or without chemotherapy in pharyngeal cancer. Clin Cancer Res 2009;15:5861-8.
34. La TH, Filion EJ, Turnbull BB, Chu JN, Lee P, Nguyen K, et al. Metabolic tumor volume predicts for recurrence and death in head-and-neck cancer. Int J Radiat Oncol Biol Phys 2009;74:1335-41.
35. Benjaminsen IC, Brurberg KG, Ruud EB, Rofstad EK. Assessment of extravascular extracellular space fraction in human melanoma xenografts by DCE-MRI and kinetic modeling. Magn Reson Imaging 2008;26:160-70.
36. Koh TS, Ng QS, Thng CH, Kwek JW, Kozarski R, Goh V. Primary colorectal cancer: Use of kinetic modeling of dynamic contrast-enhanced CT data to predict clinical outcome. Radiology 2013;267:145-54.
37. Chin SC, Lin CY, Huang BS, Tsang NM, Fan KH, Ku YK, et al. Pretreatment dynamic contrast-enhanced MRI improves prediction of early distant metastases in patients with nasopharyngeal carcinoma. Medicine (Baltimore) 2016;95:e2567.

Supplementary Table 1: Magnetic resonance imaging sequences parameters used for positron emission tomography/magnetic resonance imaging

	Region	Sequence	TR	TE	ST	FOV	VS	PAT	T
Precontrast	Whole body	Dixon VIBE AC	3.6	1.23		500	4.1×2.6×3.1	2	01:35
	Whole body	Ax T2 HASTE	1000	84	6	380	1.5×1.2×6.0	2	03:00
	Whole body	Sag STIR	3400	57	4	260	1.4×1.0×4.0	2	04:25
	Head/neck	Dixon VIBE AC	3.6	1.23		500	4.1×2.6×3.1	2	00:19
	Head/neck	Cor T1 TSE	528	12	4	300	1.2×0.9×4.0	2	01:28
	Head/neck	Cor T2 TSE FS	4300	83	4	300	1.1×0.9×4.0	2	02:45
	Head/neck	Ax T1 TSE	580	11	4	200	0.9×0.8×4.0	2	01:32
	Head/neck	Ax T2 TSE FS	5730	87	4	200	0.8×0.6×4.0	2	03:11
	Head/neck	Ax DWI	7300	62	5	256	2.0×2.0×5.0	2	2:48
Postcontrast	Head/neck	Ax DCE MRI	3.73	1.16	5	256	2.0×2.0×5.0	2	05:04
	Head/neck	Cor T1 TSE FS	679	11	4	300	1.2×0.9×4.0	2	01:53
	Head/neck	Ax T1 TSE FS	520	9.7	4	200	0.8×0.6×4.0	2	02:14
	Whole body	Ax T1 VIBE FS	4.56	1.95	3	400	1.9×1.4×3.0	2	01:12

TR: Repetition time (ms), TE: Echo time (ms), ST: SLICE thickness (mm), FOV: Field of view (mm), VS: Voxel size (mm), PAT: Parallel acquisition technique, T: Scanning time (min), VIBE: Volumetric interpolated breath-hold examination, AC: Attenuation correction, HASTE: Half-Fourier single-shot turbo spine echo, STIR: Short tau inversion recovery, TSE: Turbo spin echo, FS: Fat saturation, DWI: Diffusion-weighted imaging, DCE: Dynamic contrast-enhanced, MRI: Magnetic resonance imaging

Supplementary Table 2: Values of different positron emission tomography and magnetic resonance imaging parameters measured in the study

Parameter	Unit	Value
PET/MRI SUV_{max}	g/mL	7.82±3.07
PET/MRI MTV	cm^3	14.07±16.60
PET/MRI TLG	g/mL × cm^3	131.18±228.25
PET/CT SUV_{max}	g/mL	7.92±3.03
PET/CT MTV	cm^3	16.43±20.60
PET/CT TLG	g/mL × cm^3	170.18±365.61
K^{trans} (×10^3)	min^{-1}	348.55±575.80
k_{ep} (×10^3)	min^{-1}	161.57±211.08
v_e (×10^3)		298.04±162.28
iAUC	mm^2/s	974.96±419.70
ADC	mm^2/s	805.04±361.20

Data are expressed as means±SDs. PET: Positron emission tomography, MRI: Magnetic resonance imaging, CT: Computed tomography, SUV_{max}: Maximum standardized uptake value, MTV: Metabolic tumor volume, TLG: Total lesion glycolysis, iAUC: Initial area under the enhancement curve, K^{trans}: Volume transfer constant, k_{ep}: Flux rate constant, v_e: Extracellular volume ratio, ADC: Apparent diffusion coefficient, SDs: Standard deviations

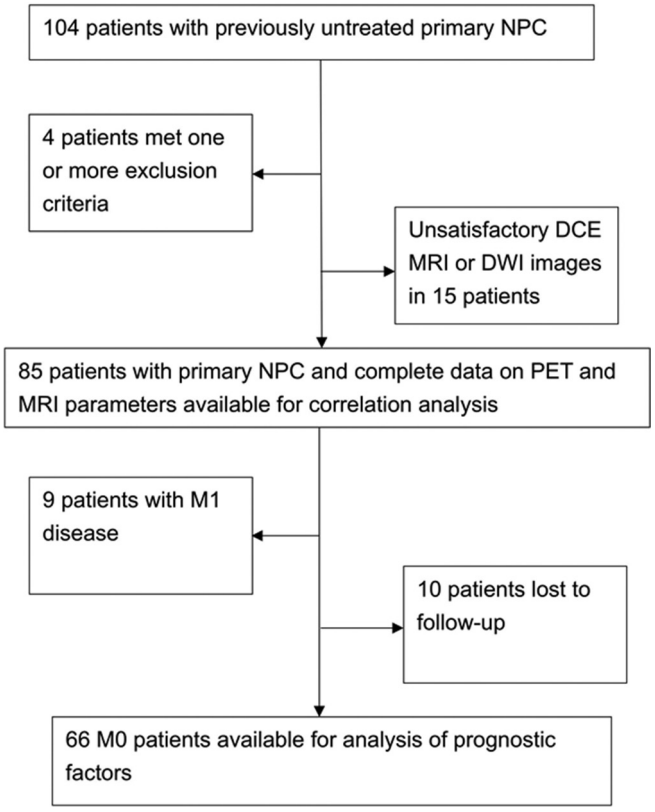

Supplementary Figure 1: The flow chart of this study

Supplementary Table 3: Correlation analysis of positron emission tomography/magnetic resonance imaging and positron emission tomography/computed tomography parameters

	PET/MRI				PET/CT			
	SUV_{max}	SUV_{mean}	MTV	TLG	SUV_{max}	SUV_{mean}	MTV	TLG
PET/MRI								
SUV_{max}	1.000							
SUV_{mean}	0.908 (<0.001)	1.000						
MTV	0.483 (<0.001)	0.421 (<0.001)	1.000					
TLG	0.578 (<0.001)	0.559 (<0.001)	0.938 (<0.001)	1.000				
PET/CT								
SUV_{max}	0.767 (<0.001)	0.674 (<0.001)	0.602 (<0.001)	0.646 (<0.001)	1.000			
SUV_{mean}	0.669 (<0.001)	0.669 (<0.001)	0.630 (<0.001)	0.669 (<0.001)	0.906 (<0.001)	1.000		
MTV	0.506 (<0.001)	0.456 (<0.001)	0.937 (<0.001)	0.941 (<0.001)	0.671 (<0.001)	0.649 (<0.001)	1.000	
TLG	0.496 (<0.001)	0.472 (<0.001)	0.846 (<0.001)	0.934 (<0.001)	0.681 (<0.001)	0.685 (<0.001)	0.953 (<0.001)	1.000

Data are expressed as correlation coefficients (Pearson's r) and corresponding *P* values in parentheses; *r* (*P* value). PET: Positron emission tomography, MRI: Magnetic resonance imaging, CT: Computed tomography, SUV: Standardized uptake value, SUV_{max}: Maximum SUV, SUV_{mean}: Mean SUV, MTV: Metabolic tumor volume, TLG: Total lesion glycolysis

Supplementary Table 4: Prediction rates of positron emission tomography/magnetic resonance imaging parameters for treatment failure

Parameter	Cutoff	Sensitivity	Specificity	PPV	NPV	AUC
SUV_{max}	18.9	57.14	57.69	26.67	83.33	0.530
MTV	14	57.14	75.00	38.10	86.67	0.640
K^{trans} ($\times 10^3$)	380	35.71	84.62	38.46	83.02	0.567
k_{ep} ($\times 10^3$)	180	35.71	86.54	41.67	83.33	0.501
v_e ($\times 10^3$)	296	64.29	65.38	33.33	87.18	0.622
iAUC	1000	42.86	57.69	21.43	78.95	0.544
ADC	767	85.71	30.77	25.00	88.89	0.582

SUV_{max}: Maximum standardized uptake value, MTV: Metabolic tumor volume, iAUC: Initial area under the enhancement curve, K^{trans}: Volume transfer constant, k_{ep}: Flux rate constant, v_e: Extracellular volume ratio, ADC: Apparent diffusion coefficient, PPV: Positive predictive value, NPV: Negative predictive value, AUC: Area under curve